Applied Energy 158 (2015) 609–618

Contents lists available at ScienceDirect

Applied Energy

journal homepage: www.elsevier.com/locate/apenergy

Improved particle swarm optimization for maximum power point tracking in photovoltaic module arrays

Kuei-Hsiang Chao *, Yu-Sheng Lin, Uei-Dar Lai

Department of Electrical Engineering, National Chin-Yi University of Technology, No. 57, Sec. 2, Zhongshan Rd., Taiping Dist., Taichung 41170, Taiwan

HIGHLIGHTS

- This study proposed an improved PSO algorithm for MPPT in PV module arrays.
- A MPPT that incorporated shading and failure conditions in PV array is developed.
- The proposed MPPT method was built using improved particle swarm optimization.
- The proposed PSO algorithm can perform MPPT for multi-peak *P–V* characteristic curves.
- The proposed PSO algorithm exhibited superior tracking speed, response, and accuracy.

ARTICLE INFO

Article history:
Received 27 January 2015
Received in revised form 2 August 2015
Accepted 15 August 2015
Available online 14 September 2015

Keywords:
Maximum power point tracking
Particle swarm optimization
Partial module shading
Module failure

ABSTRACT

In this paper, a maximum power point tracking (MPPT) method that incorporated shading and failure conditions in photovoltaic (PV) module arrays is developed. This MPPT method was built using improved particle swarm optimization (PSO). The PSO algorithm enables PV module arrays to perform MPPT for multi-peak power–voltage (*P–V*) output characteristic curves when shading or failures occur. This facilitates the tracking of actual maximum power points in PV module arrays. The HIP 2717 PV module produced by SANYO Electric Co., Ltd. was used in this study to assemble various array configurations. The characteristic curves of these array configurations when partial module shading or failure occurred were investigated. Numerous working conditions were selected for dual-peak, three-peak, and four-peak characteristics. PIC microcontrollers were then used to apply both the traditional and the proposed PSO algorithms to enable MPPT. A comparison of the measurement results showed that the proposed PSO algorithm exhibited superior tracking speed, response, and accuracy, compared with those of the traditional PSO algorithm.

1. Introduction

Photovoltaic (PV) power generation systems are composed of PV module arrays, power conditioners, and power transmission and distribution systems. Irradiation and environmental temperature changes directly affect the output power of PV module arrays, resulting in significant variations. Therefore, maximum power point tracking (MPPT) technology must be used to control PV module arrays to maximize power output. The majority of early MPPT methods have emphasized the use of traditional techniques [1–5], such as voltage feedback [1] and the constant voltage [2], power feedback [3], perturb and observe [4], and the incremental conductance methods [5]. However, these traditional MPPT methods are inappropriate for working conditions in which partial module shading or failures can occur in PV module arrays. This is because the power–voltage (*P–V*) characteristics of PV module arrays display dual-peak or multi-peak characteristics when partial module shading or failures occur [6–8]. Traditional MPPT methods can only track local maximum power points, but not global maximum power points.

Recently, numerous scholars have proposed intelligent MPPT methods for PV module arrays [9–20] to track maximum power points accurately and improve dynamic and steady-state tracking performance. However, these methods are applicable to MPPT only in conditions where the modules in the PV module arrays are not shaded. Multi-peak output curves occur frequently when modules in PV module arrays are partially shaded. Therefore, the development of an algorithm capable of accurately tracking maximum power points on complex and nonlinear output curves is critical. Scholars have proposed various algorithm architectures that are capable of tracking global maximum power points when modules

* Corresponding author. Tel.: +886 4 2392 4505x7272; fax: +886 4 2392 2156.
E-mail address: chaokh@ncut.edu.tw (K.-H. Chao).

http://dx.doi.org/10.1016/j.apenergy.2015.08.047
0306-2619/

are shaded. Among these, a two-stage method for tracking global maximum power points was suggested in [21]. However, when the global maximum power points are located to the left of the load line, this method could not track the maximum power points. In addition, this method is applicable only to tracking dual-peak characteristics. Another two-stage method for tracking global maximum power points was proposed in [22]. This method involved using a scanning program to determine curve regions containing global maximum power points. The program then applied the variable step size perturb-and-observe method to track the global maximum power points. However, this method must compare the maximum power points in each region before the global maximum power point can be derived, thereby limiting the tracking speed.

An MPPT algorithm built on the sequential extremum-seeking method was presented in [23]. This algorithm was built using approximate models and analysis of PV modules under different shading conditions. Staged searches are performed within the entire tracking range. Thus, this method provides higher computing efficiency compared with that of the sweeping search method. However, because this method adopts approximate models of PV module array shading characteristics, steady-state errors occur in the model and module parameters. A novel MPPT algorithm using artificial neural networks (ANNs) and fuzzy logic controllers was proposed in [24]. These ANNs are trained based on shading data obtained from the PV module arrays that use three-layer feed-forward training to determine global maximum power point voltage. Thus, this algorithm is connected to system parameters and requires the use of sunlight and temperature data to determine global maximum power points. These data are difficult to obtain because sensors must first be installed to obtain information. Other experts and scholars have proposed replacing the single module array of maximum power point trackers that have been used traditionally with multiple-tracker architecture [25]. This architecture would avoid an excessive influence on the overall system power generation when only several modules are shaded or fail. Although this method effectively increases overall power generation efficiency, numerous direct current (DC)–DC converters must be used, which raises equipment costs. Several papers [26,27] have been proposed to improve the dynamic and steady state responses of MPPT by adaptively tuning tracking step size. Although these methods can successfully improve the dynamic and steady state tracking performance at a specific scaling factor, an optimal scaling factor is difficult to determine due to the scaling factor is not the same under different operation conditions. In [28], a monotonically decreased tracking step size was adopted to track the exact maximum power point, but the implementation of this technique is rather complex. Some soft computing methods [29–31] are developed for MPPT algorithm under fast changing environments. These methods can rapidly calculate current maximum power points, but highly complex calculations are required. Therefore, they are not suitable for practical application. In [32], chaos search method was proposed to accurately track the global maximum power point. However, experimental results did not verify the effectiveness of this method.

Recently, various scholars have presented MPPT techniques for PV module arrays based on PSO algorithms [33–38] to improve dynamic response speed. However, the characteristics of modules under partial shading were not considered in [33]. Thus, the method by [33] is applicable for MPPT only when all modules are under identical sunlight conditions. Although the method in [34] tracks global maximum power points effectively under conditions of varying amounts of shade, this method can be applied only to systems containing multiple converters. In addition, although the method in [35] can track global maximum power points with multi-peak characteristic curves, the learning factors and weight values in the algorithm are fixed. Thus, tracking performance lacks robustness, causing low success rates in the tracking of global maximum power points with limited iteration numbers. When maximum power points are tracked successfully, the dynamic response speed is slow. Improved PSO algorithms were presented in [36–38]. The method proposed by [36] lacks system design criteria and practical design considerations. Reference [37,38] improved the traditional PSO algorithm for application to shaded PV module arrays. However, the linear decreasing method was used for parameter selection in this PSO algorithm. This parameter selection is not optimized for PV module arrays with nonlinear characteristics, particularly characteristics that occur under shaded conditions.

Therefore, in this study, the parameters of a retentive PSO algorithm [39] were adjusted using nonlinear methods to shorten tracking time and develop an MPPT method that is superior to the traditional MPPT methods used in PV module arrays under conditions of partial module shading or failure. The proposed method showed increased effectiveness in MPPT when multi-peak *P–V* characteristic curves appeared in the PV module arrays.

2. Shading and failure characteristics in PV module arrays

Arrays composed of HIP 2717 PV modules [40] that are produced by SANYO Electric Co., Ltd. were the test objects in this study. Table 1 shows the electrical specifications of these modules under standard testing conditions (AM1.5, sunlight intensity of 1000 W/m^2 and PV module temperature of 25 °C).

2.1. PV module simulator circuitry

To facilitate experimentation on PV module array shading and failure characteristics, an HIP 2717 PV module simulator containing adjustable partial shadow and failure circuitry was used, as shown in Fig. 1 [41]. The circuit architecture comprised a Darlington pair amplification circuit, an output current limiter, and a voltage stabilization circuit to enable implementation of PV modules containing various shading characteristics. Variable resistors VR_{Isc} and VR_{Voc} were adjusted to possess both open-circuit voltage and short-circuit current output characteristics at various shade ratios. The R_B and VR_{Voc} divider circuits were used to adjust shade ratios. When a V_{PV} power supply is not provided, the PV module simulator does not contain output power; this is equivalent to setting the PV module to failure conditions.

The BJT transistor 2N3055, with ratings of I_C = 15 A, V_{CEO} = 60 V, P_{tot} = 115 W, and h_{FE} = 20, was chosen for the output transistor Q_2. Then, the 2N2219, with ratings of I_C = 0.8 A, P_{tot} = 3 W, V_{CEO} = 30 V, and h_{FE} = 20, was chosen for Q_1 to form a Darlington amplifier with Q_2. Accordingly, the 2N1815, with ratings of I_C = 150 mA, P_{tot} = 400 mW, V_{CEO} = 50 V, and I_B = 50 mA, was chosen for Q_3 and Q_4 to serve as the base current driver of Q_1.

In the PV module simulator circuit, the resistance values of R_A, R_B, R_C and R_D are given 2 kΩ, 2 kΩ, 2 Ω, and 510 Ω, respectively. According to the shadow ratios of a PV module, the open-circuit voltage, V_{oc}, and short-circuit current, I_{sc}, can be determined according to their *I–V* characteristic curves, using either a

Table 1
Electrical specifications of the SANYO HIP 2717 PV modules.

Maximum output power (P_{mp})	27.8 W
Maximum power point current (I_{mp})	1.63 A
Maximum power point voltage (V_{mp})	17.1 V
Short-circuit current (I_{sc})	1.82 A
Open-circuit voltage (V_{oc})	21.6 V
Module length and width specifications	496 mm × 524 mm

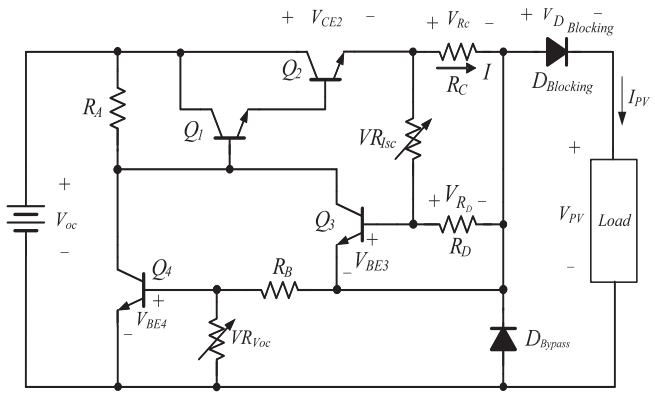

Fig. 1. PV module simulator circuitry.

simulation or experiment. Therefore, the values of VR_{Isc} and VR_{Voc} in the proposed PV module simulator can be determined for shadow ratios ranging from 0% to 80%. In the PV module simulator circuit, variable resistors of 5 kΩ and 1 kΩ are chosen for VR_{Isc} and VR_{Voc}, respectively.

2.2. Analysis of PV module array series and parallel characteristics

2.2.1. Characteristics in conditions without shading or failure

In a M-series N-parallel PV module array without shading or failure, if the power point voltage, maximum power point current, and maximum power point of a single PV module are represented by V_{mp}, I_{mp}, and P_{mp}, respectively, then the maximum power point voltage of the M-series N-parallel array is $M \times V_{mp}$, the maximum power point current is $N \times I_{mp}$, and the maximum power point is $M \times N \times P_{mp}$.

2.2.2. Characteristics in conditions with shading or failure

When modules in the module array fail, the modules form loops through bypass diodes to maintain some generating capacity in the PV module array. Although these diodes improve the output power reductions exhibited when several modules fail, the diodes cannot improve the reductions in output voltage and current that occur when modules are shaded. In addition, when the PV module-shading ratio becomes excessively high, the output power exhibits dual or multiple peaks. This prevents MPPT from controlling the module arrays to operate at the actual maximum power points.

Because of these characteristics in actual PV module arrays, a SANYO HIP 2717 module simulator [40] was used in this study. The simulator was set to various shade ratios and failure conditions to assemble PV module arrays with different series–parallel configurations for MPPT testing. Fig. 2 shows a four-series one-parallel P–V array characteristic composed of SANYO HIP 2717 PV modules. These P–V characteristic curves were obtained at 30% shading conditions (sc) for different numbers of shaded modules. The figure shows that multiple peaks occurred in the P–V characteristic curve when partial shading occurred on several array modules. When failure occurred in the PV module array, each module that failed lost the ability to function and did not output electric current to supply the load. The electric current from the working modules flowed through the bypass diode of the failed modules, thereby enabling the working modules to continue functioning normally. Fig. 3 presents the P–V output characteristic curves for different numbers of failed modules. The figure shows that multiple peaks did not occur in the P–V characteristic curves when some modules of the same series array failed.

3. MPPT method using the traditional and proposed PSO algorithm

Kennedy and Eberhart proposed the PSO algorithm in [39]. This concept originates from group-behavior theory and was inspired by the observation that groups of birds and fish pass messages between individual members to enable the entire group to move forward toward the same objects and directions. The PSO algorithm imitates this biological behavior when seeking benefit-maximization methods for an entire group.

3.1. MPPT method using the traditional PSO algorithm

The steps of the traditional PSO algorithm are as follows.

Step 1: Set the number of particles P and the iteration numbers N.

Step 2: Initialize the value of each particle (in this study, this is duty cycle D of the boost converter). Begin initial movement speed V_i^j for each particle. Initialize the individual optimal D value P_{best} (i.e., the initial D value) for each particle. Initialize the optimal D value G_{best} for all particles.

Step 3: Given cognition-only learning factor C_1, social-only learning value C_2, and inertia weight W, insert the initial D values for each particle into (1) to obtain the newest speed. Update the D value in (2).

$$V_i^{j+1} = W \times V_i^j + C_1 \times rand1(\cdot) \times (P_{best,i} - P_i^j) + C_2 \times rand2(\cdot) \times (G_{best} - P_i^j) \quad (1)$$

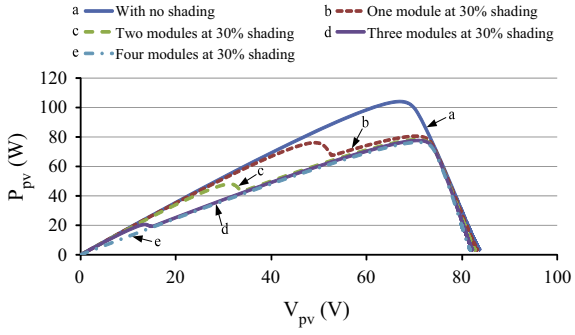

Fig. 2. P–V characteristic curves of the four-series one-parallel system under normal operating conditions and under 30% shading conditions when various numbers of modules failed.

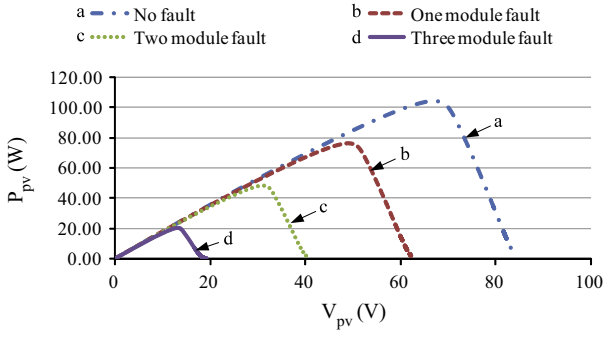

Fig. 3. P–V characteristic curves of the four-series one-parallel system under normal operating conditions and under conditions when various numbers of modules failed.

$$P_i^{j+1} = V_i^{j+1} + P_i^j \quad (2)$$

Step 4: Compare the power values produced by P_i^{j+1} and P_i^j at the D value and substitute the larger value for $P_{best,i}$.
Step 5: Compare the power values produced by $P_{best,i}$ and G_{best} at the D value and substitute the larger value for G_{best}.
Step 6: Repeat Steps 3–5 until completing the set number of iterations.

The relevant parameters used in traditional PSO are explained as follows.

Number of particles: P represents the number of points tracked at different initial duty cycle D values.
Iteration number: N denotes the number of times each particle moves.
Cognition-only learning factor: C_1 represents the learning parameters associated with individual particles.
Social-only learning factor: C_2 denotes the learning parameters associated with other particles.
Inertia weight: W represents the correlation with the most recent particle movement distance.
V_i^j: This variable represents the movement speed of the ith particle during the jth iteration.
P_i^j: This variable denotes the duty cycle D value for the ith particle during the jth iteration.
*Rand*1(·): This variable represents a value between 0 and 1 generated by the first random number generator.
*Rand*2(·): This variable denotes a value between 0 and 1 generated by the second random number generator.
$P_{best,i}$: This denotes the optimal duty cycle D value for the ith particle.
G_{best}: This variable represents the optimal duty cycle D value for all particles.

In general, C_1, C_2, and W in the traditional PSO algorithm are fixed values set to $W = (10 - C_1 - C_2)/10$.

3.2. MPPT method using the proposed PSO algorithm

A traditional PSO-based MPP tracker has been specifically designed to track the global MPP on a characteristic curve with multiple peaks, but in the absence of robustness, since all the weights remain constant during the entire iterative process. In other words, it gives a low probability that the MPP can be successfully tracked within a specified number of iterations, and gives a slow dynamic response in a successful MPP tracking event. In view of this, this work is proposed as an improved version of typical tracking algorithms when dealing with the global MPP tracking issue experienced in an array involved partially shaded or even malfunctioning PV modules.

The proposed PSO algorithm involves adjusting Step 3 of the traditional PSO. Variables C_1, C_2, and W were altered to calculate (3)–(5) to obtain linear changes; thus, C_1, C_2, and W vary for each iteration.

$$C_1 = C_{1,max} - (C_{1,max} - C_{1,min}) \times \frac{2^j + 1}{2^N + 1} \quad (3)$$

$$C_2 = C_{2,min} + (C_{2,max} - C_{2,min}) \times \frac{2^j + 1}{2^N + 1} \quad (4)$$

$$W = W_{max} - (W_{max} - W_{min}) \times \frac{2^j + 1}{2^N + 1} \quad (5)$$

The parameters added for the proposed PSO are explained as follows.

Cognition-only learning factor upper limit: $C_{1,\max}$ represents the upper limit to the learning parameters associated with the particles.
Cognition-only learning factor lower limit: $C_{1,\min}$ denotes the lower limit to the learning parameters associated with the particles.
Social-only learning factor upper limit: $C_{2,\max}$ represents the upper limit to the learning parameters associated with other particles.
Social-only learning factor lower limit: $C_{2,\min}$ denotes the lower limit to the learning parameter associated with other particles.
Inertia weight upper limit: W_{max} represents the upper limit to the correlation with movement distances of individual particles.
Inertia weight lower limit: W_{min} denotes the lower limit to the correlation with movement distance of individual particles.

For example, if $C_{1,max} = 4$, $C_{1,min} = 1$, $C_{2,max} = 4$, $C_{2,min} = 1$, $W_{max} = 0.8$, $W_{min} = 0.2$, and N = 10, (3)–(5) can be calculated to change C_1, C_2, and W (shown in Fig. 4). The figure shows that C_1 and W in the proposed PSO decreased when the iteration number increased, which indicates that the ability to reference the optimal positions of the individual particles decreased when the iteration number increased. However, C_2 increased when the iteration number increased, indicating that the global optimal particle reference results gained more weight when the iteration number increased.

The steps for the proposed PSO algorithm are nearly identical to those of the traditional PSO algorithm. The proposed algorithm only differs because (3)–(5) are adopted for the C_1, C_2, and W parameters in Step 3 to enable adjustments according to the iteration number.

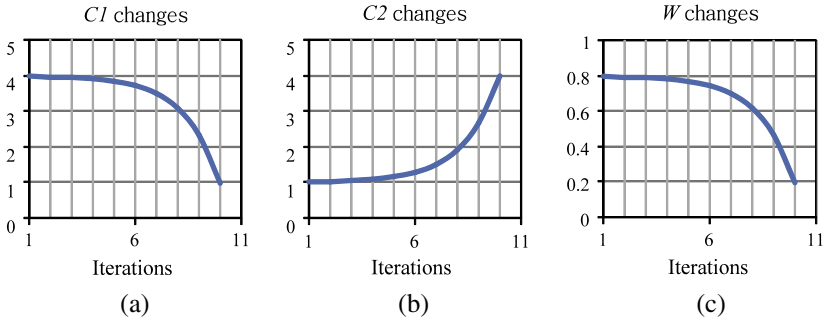

Fig. 4. Parameter value changes in the proposed PSO: (a) C_1; (b) C_2; (c) W.

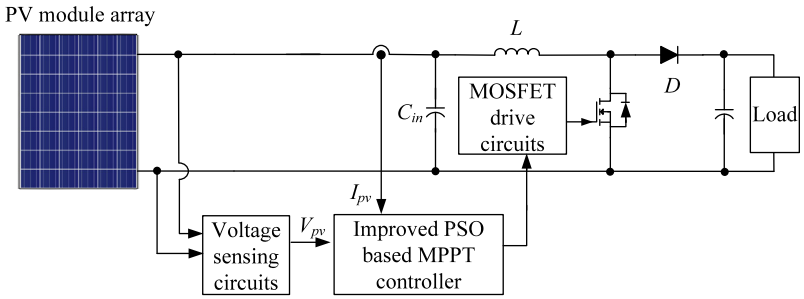

Fig. 5. Proposed PSO maximum power tracking controller architecture.

Table 2
Rated component-design values of the DC/DC boost converter.

Element names	Specifications
Inductor (L)	1 mH
Capacitor (C_{in})	47 0μF/450 V
Capacitor (C_{out})	470 μF/450 V
Switching frequency (f)	20 kHz
Transistor	IRF460 (500 V/20 A)
Diode	DSEP30-12A (1200 V/30 A)

3.3. MPPT scheme using the traditional and proposed PSO method

Fig. 5 presents the maximum power point tracker architecture based on the traditional and proposed PSO algorithm for the PV module arrays. This architecture contained two main subsystems: (1) a DC/DC boost converter and (2) an traditional or the proposed PSO MPPT controller. Using the traditional and proposed PSO steps described in Subsection 3.1 and 3.2, the PV module array system applied the traditional and proposed PSO maximum power point controller to control the duty cycle of the boost converter. This enabled the PV module array to output maximum power despite that several modules had been partially shaded or had failed.

Table 2 presents the component parameter values for the DC/DC boost converter circuitry used in this study [42]. Tables 3 and 4 show the relevant parameters for the traditional and proposed PSO algorithms, respectively. Table 5 depicts the PV module array tests performed under six working conditions. Testing was performed in accordance with the PSO algorithm steps shown in Section 3.

Table 3
Parameter settings of the traditional PSO algorithm.

Parameter name	Parameter values
Particle number (P)	3
Iterations (N)	30
Cognition-only learning factor (C_1)	3
Social-only learning factor (C_2)	3
Inertia weigh (W)	0.4

Table 4
Parameter settings of the proposed PSO algorithm.

Parameter name	Parameter values
Particle number (P)	3
Iterations (N)	30
Cognition-only learning factor upper limit ($C_{1,max}$)	3
Cognition-only learning factor lower limit ($C_{1,min}$)	1
Social-only learning factor upper limit ($C_{2,max}$)	3
Social-only learning factor lower limit ($C_{2,min}$)	1
Inertia weigh upper limit (W_{max})	0.8
Inertia weigh lower limit (W_{min})	0.4

Table 5
Selected indicative test cases.

Case	Partial shading or failure conditions	Number of P–V curve peaks
1	1-series 1-parallel: 0% shading	1
2	2-series 2-parallel: 0% shading + 0% shading + 0% shading + 0% shading	1
3	4-series 1-parallel: 0% shading + 0% shading + 30% shading + 50% shading	3
4	4-series 1-parallel: 0% shading + 30% shading + 50% shading + 70% shading	4
5	4-series 1-parallel: 50% shading + failure + 30% shading + 0% shading	3
6	2-series 2-parallel: (0% shading + 0% shading) // (failure + 0% shading)	2

Note: The symbol + represents the series connections and the symbol // represents parallel connections.

The PIC181F8720 microprocessor manufactured by Microchip Technology was used to implement the conventional PSO method in the empirical test. First, the parameter values in the iteration formula of Table 3 were set, with the iteration number being set to zero. The initial position of each particle was set randomly (i.e., duty cycle of the boost converter). The PWM control signal with this initial value was transmitted to the boost converter to activate a power semiconductor switch. Subsequently, the output voltage and current values of the PV module array were extracted using a sensor and transmitted to the microcontroller through the analog-to-digital converter to calculate the power value. Subsequently, the initially settings are described as follows. The calculated power value and particle position (duty cycle of the boost converter) were predetermined as the $P_{best,i}$ and V_i^j of the first iteration, respectively. The highest power of a particle among all of the particles and the relative position of the particle (duty cycle) were set to be the G_{best} and V_i^j of the first iteration. The aforementioned settings were substituted into the PSO kernel iteration formula, increasing each iteration number by 1. If a particle attained a power value exceeding that of the $P_{best,i}$ value after a duty cycle update, then the $P_{best,i}$ and V_i^j values would be updated. If any of the particles attained a power value higher than that of the G_{best} value, then the G_{best} and V_i^j values would be updated, completing the iteration. These steps were repeated until the maximal iteration number was achieved. The iteration process of the proposed PSO method was realized using a process identical to that of the conventional PSO method, except that the adjustment of parameter values in the iteration formula were adjusted according to Table 4 and (3)–(5).

4. Measurement results for the traditional PSO and proposed PSO tracking methods

This section presents the measurements of the characteristic curves for the six working conditions shown in the PV module

simulator circuitry composition table in Fig. 1 under various shading ratios and failure conditions. PIC microcontrollers were used to implement the traditional and proposed PSO MPPT methods. The tracking performances were compared.

4.1. Characteristic curves under six working conditions

Figs. 6–11 present the current–voltage (*I–V*) and *P–V* characteristic curves measured under the six working conditions that were depicted in Table 5. Figs. 6 and 7 show that short-circuit current I_{sc} did not change when two PV modules were connected in a series, although the open-circuit voltage V_{oc} doubled. When connected in parallel, the open-circuit voltage V_{oc} did not change, whereas the short-circuit current I_{sc} doubled. Therefore, in conditions at fixed temperatures, fixed irradiation, and without partial shading or failure, the size of the open-circuit voltage V_{oc} in the PV module array and the number of series modules were proportional. Short-circuit current I_{sc} was also proportional to the number of parallel modules and multiple peaks did not occur in the *P–V* characteristic curves. Figs. 8 and 9 indicate that *N* number of peaks occurred in the *P–V* characteristic curve when *N* modules received different ratios of shade within the same series. Fig. 10 indicates that the *P–V* characteristic curves were unaffected by failure and presented *N* number of peaks when module failure occurred within a single series in an array and *N* modules were tested using different ratios of shade. Fig. 11 presents two-series two-parallel module array

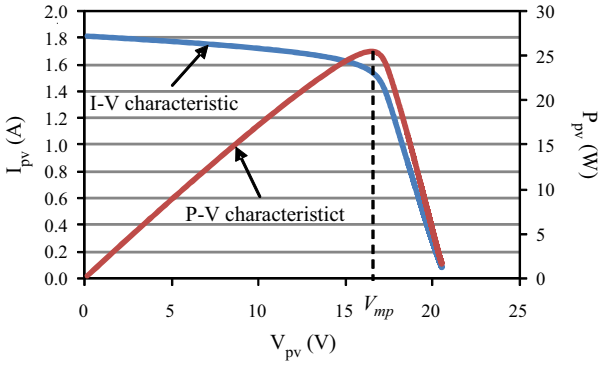

Fig. 6. The *I–V* and *P–V* characteristic curves for a one-series one-parallel module array without shading or failure.

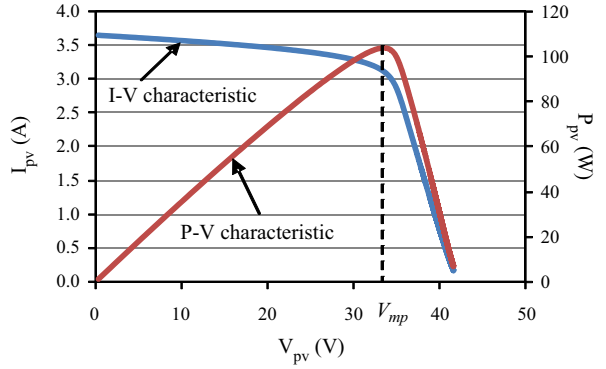

Fig. 7. The *I–V* and *P–V* characteristic curves for a two-series two-parallel module array without shading or failure.

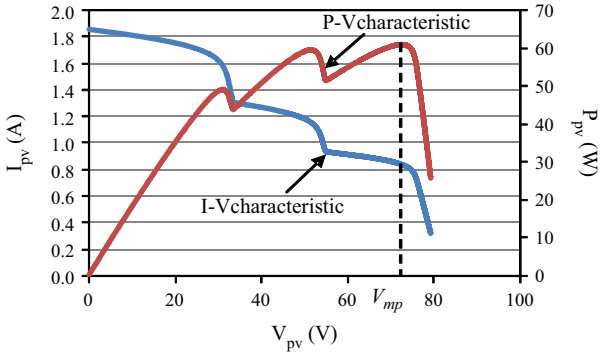

Fig. 8. The *I–V* and *P–V* output characteristics under conditions of 0% shading + 0% shading + 30% shading + 50% shading in a four-series one-parallel module array.

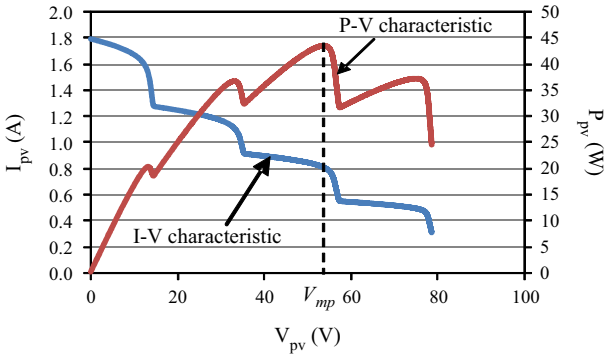

Fig. 9. The *I–V* and *P–V* output characteristics under conditions of 0% shading + 30% shading + 50% shading + 70% shading in a four-series one-parallel module array.

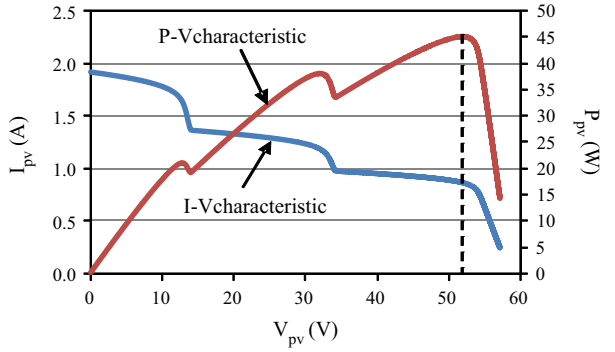

Fig. 10. The *I–V* and *P–V* output characteristics under conditions of 50% shading + failure + 30% shading + 0% shading in a four-series one-parallel module array.

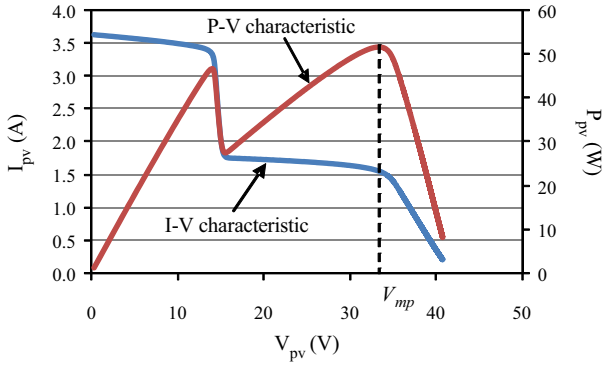

Fig. 11. The *I–V* and *P–V* output characteristics under conditions of (0% shading + 0% shading) // (failure + 0% shading) in a two-series two-parallel module array.

configurations with all modules not shaded in one series and failure in one module in the other series. In this connection configuration, although three modules were not shaded and only one module failed, two peaks appeared in the *P–V* characteristic curve.

4.2. PV module array MPPT measurements

In this study, the measured waveforms were power characteristic curves that were obtained by using Excel to multiply voltage and current signals after recording the voltage and current data from the module arrays. This section presents how observations were performed and how the advantages and disadvantages of the two measured waveforms were compared to facilitate future comparisons of the traditional PSO and proposed PSO measurement results.

For example, the horizontal timeline shown in Fig. 12 contains two intervals: $t_0 - t_1$ and $t_1 - t_2$. The time between t_0 and t_1 was the preparation time for the duty cycle to approach 0. At this time, the voltage approached the open-circuit voltage and the current was extremely low. Because a fixed duty cycle was adopted, the voltage, current, and power were all fixed values. The time between t_1 and t_2 was the time required by the duty cycle to change from the 1st iteration to the 30th iteration. To facilitate observation of these altered results, this time was extended by a short period after the duty cycle changed for each iteration. Therefore, the total time required for the 30 iterations was approximately 0.12 s and the average iteration time was approximately 0.004 s (=0.12/30 = 4 ms). The time between t_1 and t_2 indicates that the voltage, current, and power changed following alterations in the duty cycle. At this time, power increased rapidly from P_1 to P_a, only requiring $(t_a - t_1)$ time. The interval in which power increased from P_a to P_b was $(t_b - t_a)$ time. Beginning at t_b, the power curve tended to gradually move toward a stable value until stopping at t_2.

The results in Fig. 12 indicate that short $(t_a - t_1)$ time represented increased speeds in power tracking from P_1 to P_a. When the power value at time t_b approached the power value at time t_2, this indicated that the MPPT beginning at t_b was gradually stabilizing. These methods were used to observe and compare the performance advantages and disadvantages of the traditional and proposed PSO methods. The performance was based on whether

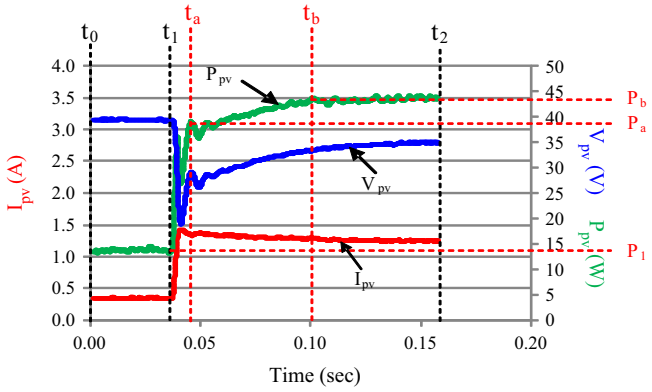

Fig. 12. Voltage, current, and power response waveforms for the PV module arrays during MPPT.

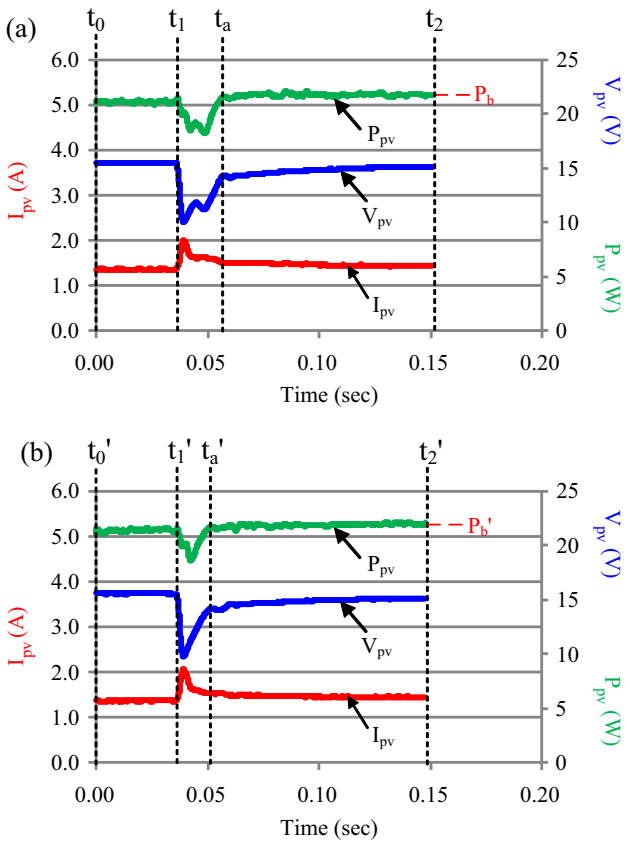

Fig. 13. Measurement results from a one-series one-parallel module array without shading: (a) traditional PSO method (P_{mp} = 21.74 W); (b) proposed PSO method (P_{mp} = 21.95 W).

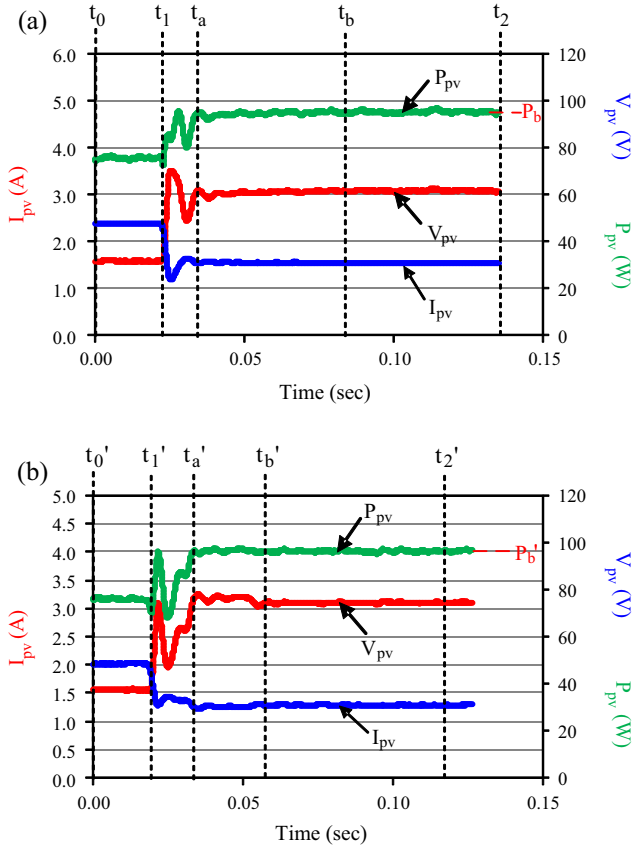

Fig. 14. Measurement results from a two-series two-parallel module array without shading: (a) traditional PSO method (P_{mp} = 95.64 W); (b) proposed PSO method (P_{mp} = 96.51 W).

increased P_b values could be tracked and which method provided the faster response speed at 30 iterations.

Fig. 13(a) and (b) show the measured response waveforms for the traditional and proposed PSO methods for Case 1, which was previously shown in Table 5. In the tracking iteration formula of the proposed PSO, the weighting (W) and learning factors (C_1 and C_2) varied as the iteration number increased. In the initial iteration period, because the working point was distant from the MPP, a high weighting and large steps were adopted for tracking MPP. In the initial tracking period, maximal power values that were tracked by individual particles exerted a considerable effect; thus, a large cognition-only learning factor (C_1), which accelerated the tracking speed of the proposed PSO method compared with that of the conventional one. As the iteration number increased, the tracked working point would gradually approach the global MPP and the effect of the individual particles' maximal power value would decrease as the effect of the global particles' maximal power value increased. Thus, the W and C_1 values were reduced, and the social-only learning factor (C_2) was added to reduce oscillations near the tracked working point, thereby improving the steady-state tracking performance of the maximal power tracker. As shown in Fig. 13(a), the tracking time of the conventional PSO required 20 ms from t_1 to t_a, whereas the tracking time required only 15 ms from t_1' to t_a' when the proposed PSO was adopted. Thus, the measured quantitative data verified that the proposed PSO had a tracking time 5 ms faster than that of the conventional PSO. After 30 iterations, the P_b' value (21.95 W) from the proposed PSO method was greater than the P_b value (21.74 W) of the traditional PSO method; therefore, the proposed PSO method exhibited superior performance. Therefore, a comparison of the results presented in Fig. 13(a) and (b) indicated that although both methods could track maximum power points, the $(t_a' - t_1')$ time obtained using the proposed PSO method was shorter than the $(t_a - t_1)$ time obtained using the traditional PSO method.

Fig. 14(a) and (b) depict the measured response waveforms for the traditional and proposed PSO methods for Case 2, which was previously shown in Table 5. In the initial iteration period, the W and C_1 values of the proposed PSO method's tracking iteration formula were increased for maximal power tracking because the working point was distant from the MPP. The effect of the individual particles' maximal power value was considerable in the initial tracking period; thus, a large cognition-only learning factor (i.e., C_1) was adopted, which enabled a faster initial tracking speed in the proposed PSO method than in the conventional one. As the iteration number increased, the tracked working points increased and gradually approached the MPP. In addition, the effect of the individual particles' maximal power value decreased, whereas the effect of the global particles' maximal power value increased. Thus, the W and C_1 values were reduced, and the social-only learning factor (i.e., C_2) was incorporated to reduce oscillations near the tracked working point. Consequently, the final tracked maximal power value was high. The methods for adjusting the iteration parameters of the proposed PSO are listed in Table 4 and (3)–(5). The design of the conventional PSO adopted iteration parameters with fixed values (Table 3); thus, the conventional POS method lacked robustness. The figures show that the tracking time t_a' obtained using the proposed PSO method was close to t_b' at the beginning of the test and the final maximum power value was high. Therefore, the proposed PSO method exhibited superior tracking performance compared with the traditional PSO method.

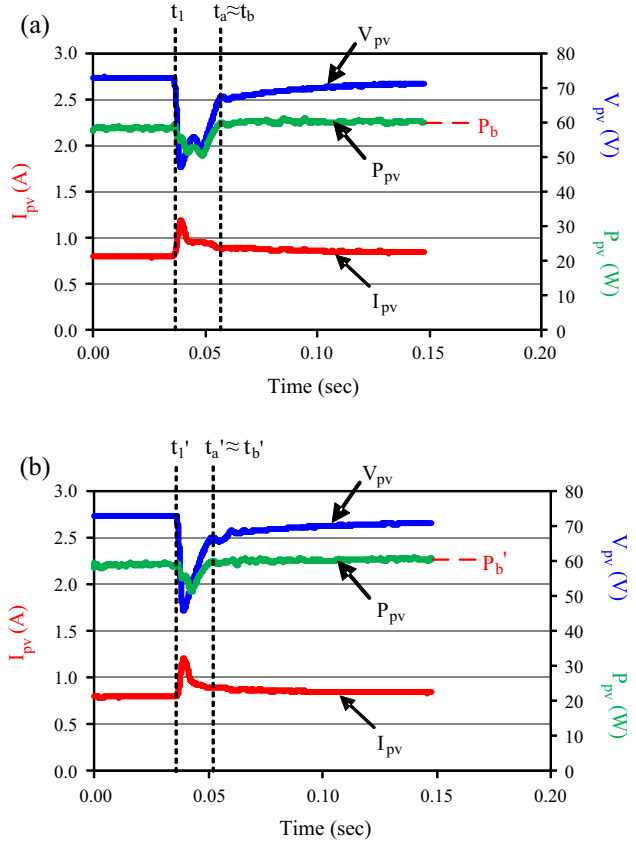

Fig. 15. Measurement results for a four-series one-parallel module array under working conditions of 0% shading + 0% shading + 30% shading + 50% shading: (a) traditional PSO (P_{mp} = 60.14 W); (b) proposed PSO (P_{mp} = 60.36 W).

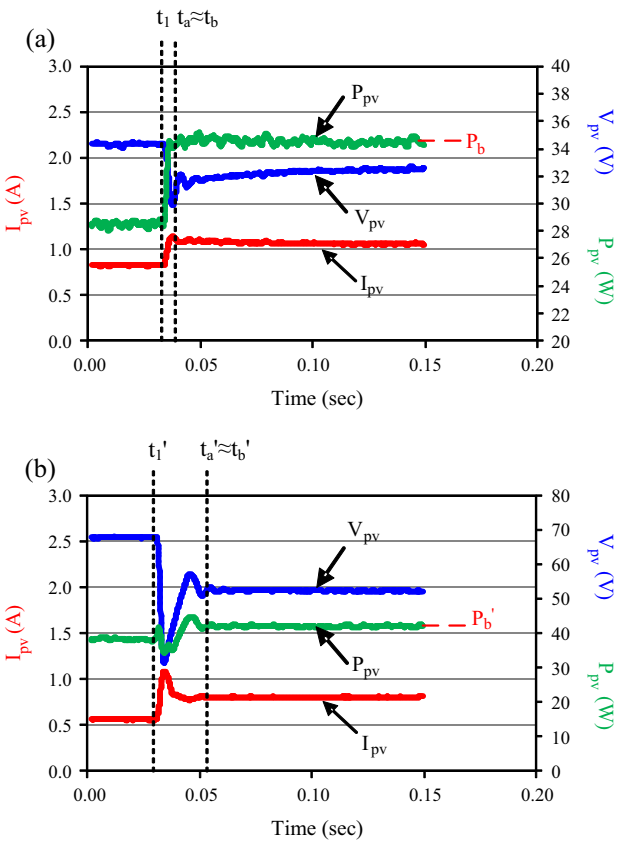

Fig. 16. Measurement results for a four-series one-parallel module array under working conditions of 0% shading + 30% shading + 50% shading + 70% shading: (a) traditional PSO (P_{mp} = 34.38 W); (b) proposed PSO (P_{mp} = 42.39 W).

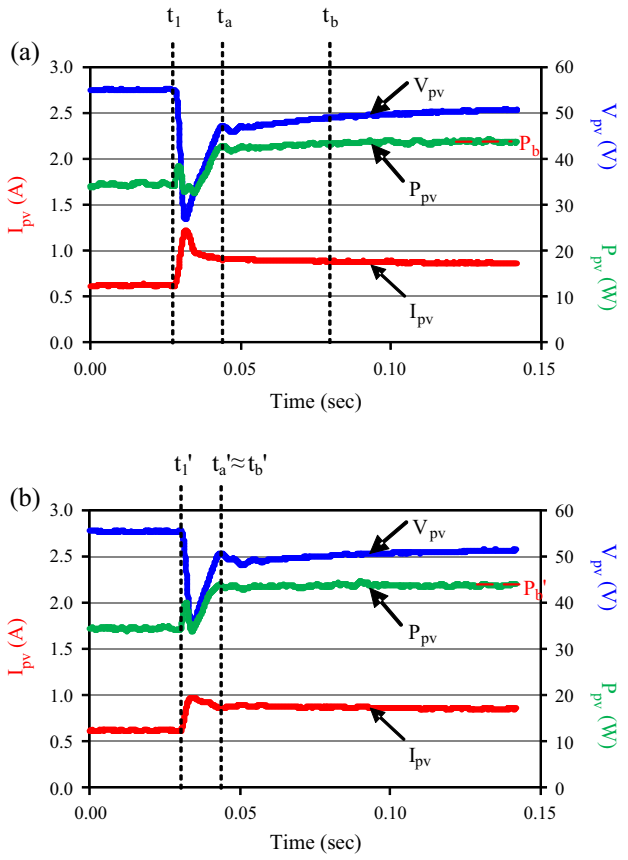

Fig. 17. Measurement results for a four-series one-parallel module array under working conditions of 50% shading + failure + 30% shading + 0% shading: (a) traditional PSO (P_{mp} = 43.66 W); (b) proposed PSO (P_{mp} = 44.01 W).

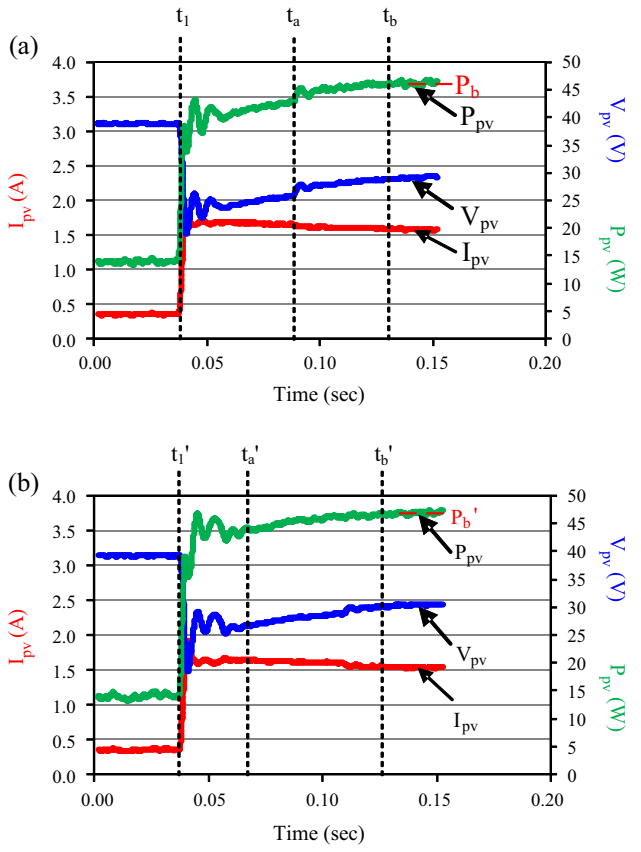

Fig. 18. Measurement results for a two-series two-parallel module array under working conditions of (0% shading + 0% shading) // (failure + 0% shading): (a) traditional PSO (P_{mp} = 46.38 W); (b) proposed PSO (P_{mp} = 47.14 W).

Figs. 15–18 depict the tracking response waveforms measured by performing MPPT using both the traditional and proposed PSO methods in module arrays containing shading or failure. Fig. 15 presents the measured waveforms for current, voltage, and power tracking in the four-series one-parallel module array for Case 3 under working conditions of 0% shading + 0% shading + 30% shading + 50% shading.

Fig. 15(a) and (b) indicate that both methods approached the maximum power point within a short period. However, $(t'_a - t'_1)$ time was shorter than $(t_a - t_1)$ time. After 30 iterations, P'_b was slightly greater than P_b. Thus, the proposed PSO method was superior to the traditional PSO method.

Fig. 16 shows the measured current, voltage, and power tracking waveforms for the four-series one-parallel module array for Case 4 under working conditions of 0% shading + 30% shading + 50% shading + 70% shading.

Fig. 16(a) and (b) indicate that the traditional PSO method was consistently trapped at local maximum power points within 30 iterations. The proposed PSO method approached the true maximum power point within the elapsed $(t'_a - t'_1)$ time. In addition, P'_b (42.39 W) was greater than P_b (34.38 W). Thus, the tracking performance of the proposed PSO was superior to that of the traditional PSO.

Fig. 17 presents the measured current, voltage, and power tracking waveforms for the four-series one-parallel module array for Case 5 under working conditions of 50% shading + failure + 30% shading + 0% shading.

Fig. 17(a) and (b) show that the $(t'_a - t'_1)$ time for the proposed PSO was shorter than the $(t_a - t_1)$ time of the traditional PSO. The initial t'_a approached t'_b. In addition, P'_b was slightly greater than P_b after 30 iterations. Therefore, the tracking performance of the proposed PSO was superior to that of the traditional PSO.

Fig. 18 presents the measured current, voltage, power tracking waveforms for the two-series two-parallel module array for Case 6 under conditions of (0% shading + 0% shading) // (failure + 0% shading).

Fig. 18(a) and (b) indicate that the initial $(t'_a - t'_1)$ time for the proposed PSO was shorter than the $(t_a - t_1)$ time for the traditional PSO. In addition, P'_b from the proposed PSO was slighter greater than P_b from the traditional PSO after 30 iterations. Therefore, the tracking performance of the proposed PSO was superior to that of the traditional PSO.

5. Conclusions

This study proposed an improved PSO algorithm for MPPT in PV module arrays. To accelerate the efficiency and performance of PSO tracking, an exponential-form parameter control method was presented. This method used exponential increases or decreases in the cognition-only learning factor, the social-only learning factor, and the inertia weight to reduce iteration numbers and improve tracking success. The results showed that the proposed PSO algorithm could track actual maximum power points faster and more accurately in PV module arrays under conditions of partial module shading or failure than could the traditional PSO algorithm. In addition, the test results from six selected partial shading or failure conditions indicated that the average iteration numbers required for successful MPPT using the proposed PSO was 21.1. By contrast, the average iteration number required for success using the

traditional PSO was 38.3. These results confirm that the proposed PSO method improved the success rate of tracking. Therefore, applying the proposed PSO method to MPPT in PV module arrays, particularly when various modules are partially shaded or have failed, is feasible.

Although various configuration arrays composed of different PV modules exhibited an identical trend in slopes, the slopes and slope variations of the *P–V* characteristic curves were dissimilar. Therefore, to improve the dynamic and steady-state performance of the maximal power tracker, the proposed PSO method can adjust the parameter values of the PSO iteration formula through online adaptive tuning, only according to the slope characteristics of the individual *P–V* characteristic curves. Therefore, relevant quantitative design methods can be discussed and analyzed in future research.

Acknowledgments

The authors gratefully acknowledge the support of the National Science Council, Taiwan, Republic of China, under the Grant NSC 102-2221-E-167-009.

References

[1] Masoum MAS, Sarvi M. Voltage and current based MPPT of solar arrays under variable insolation and temperature conditions. In: Power engineering, the 43th international universities conference on; 2008. p. 1–5.
[2] Masoum MAS, Dehbonei H, Fuchs EF. Theoretical and experimental analyses of photovoltaic systems with voltage and current-based maximum power-point pracking. Energy Convers IEEE Trans 2002;17:514–22.
[3] Esram TT, Chapman PL. Comparison of photovoltaic array maximum power point tracking techniques. Energy Convers IEEE Trans 2007;22:439–49.
[4] Femia N, Granozio D, Petrone G, Spagnuolo G, Vitelli M. Predictive and adaptive MPPT perturb and observe method. Aerosp Electron Syst IEEE Trans 2007;43:934–50.
[5] Lin CH, Huang CH, Du YC, Chen JL. Maximum photovoltaic power tracking for the PV array using the fractional-order incremental conductance method. Appl Energy 2011;88:4840–7.
[6] Patel H, Agarwal V. MATLAB-based modeling to study the effects of partial shading on PV array characteristics. Energy Convers IEEE Trans 2008;1:302–10.
[7] Wang YJ, Hsu PC. Analytical modelling of partial shading and different orientation of photovoltaic modules. Renew Power Gener IET 2010;4:272–82.
[8] Paraskevadaki EV, Papathanassiou SA. Evaluation of MPP voltage and power of mc-Si PV modules in partial shading conditions. Energy Convers IEEE Trans 2011;26:923–32.
[9] Pan CT, Chen JY, Chu CP, Huang YS. A fast maximum power point tracker for photovoltaic power systems. In: Industrial electronics conference 1999, IEC on 1999. IEEE 25th international; 1999. p. 390–3.
[10] Leyva R, Alonso C, Queinnec I, Cid-Pastor A, Lagrange D, Martinez-Salamero L. MPPT of photovoltaic systems using extremum-seeking control. Aerosp Electron Syst IEEE Trans 2006;42:249–58.
[11] Esram T, Kimball JW, Krein PT, Chapman PL, Midya P. Dynamic maximum power point tracking of photovoltaic arrays using ripple correlation control. Power Electron IEEE Trans 2006;21:1282–91.
[12] Rodriguez C, Amaratunga GAJ. Analytic solution to the photovoltaic maximum power point problem. Circuits Syst I: Regular Pap IEEE Trans 2007;54:2054–60.
[13] Fortunato M, Giustiniani A, Petrone G, Spagnuolo G, Vitelli M. Maximum power point tracking in a one-cycle-controlled single-stage photovoltaic inverter. Ind Electron IEEE Trans 2008;55:2684–93.
[14] Chao KH, Lee YH. A maximum power point tracker with automatic step size tuning scheme for photovoltaic systems. J Photoenergy Int 2012;2012:1–10.
[15] Ramaprabha R. Maximum power point tracking using GA-optimized artificial neural network for solar PV system. In: Electrical energy systems conference, first international; 2011. p. 264–8.
[16] Besheer AH. Ant colony system based PI maximum power point tracking for stand alone photovoltaic system. In: International industrial technology conference on: IEEE; 2012. p. 693–8.
[17] Adly M. An optimized fuzzy maximum power point tracker for stand alone photovoltaic systems: ant colony approach. In: Industrial electronics and applications conference on: 7th IEEE; 2012. p. 113–9.
[18] Chao KH, Chiu CL. Design and implementation of an intelligent maximum power point tracking controller for photovoltaic systems. Int Rev Electr Eng 2012;17:3759–68.
[19] Yau HT, Wu CH. Comparison of extremum-seeking control techniques for maximum power point tracking in photovoltaic systems. Energies 2011;4:2180–95.
[20] Zazo H, del Castillo E, Reynaud JF, Leyva R. MPPT for photovoltaic modules via Newton-like extremum seeking control. Energies 2012;4:2653–66.
[21] Patel H, Agarwal V. Maximum power point tracking scheme for PV systems operating under partially shaded conditions. Ind Electron IEEE Trans 2008;55:1689–98.
[22] Renaudineau H, Houari A, Martin JP, Pierfederici S, Tabar FM, Gerardin B. A new approach in tracking maximum power under partially shaded conditions with consideration of converter losses. Sol Energy 2011;85:2580–8.
[23] Lei P, Li Y, Seem JE. Sequential ESC-based global MPPT control for photovoltaic array with variable shading. Sustain Energy IEEE Trans 2011;2:348–58.
[24] Syafaruddin EK, Hiyama T. Artificial neural network-polar coordinated fuzzy controller based maximum power point tracking control under partially shaded conditions. Renew Power Gener IET 2009;3:239–53.
[25] Femia N, Lisi G, Petrone G, Spagnuolo G, Vitelli M. Distributed maximum power point tracking of photovoltaic arrays: novel approach and system analysis. Ind Electron IEEE Trans 2008;55:2610–21.
[26] Chen PC, Chen PY, Liu YH, Chen JH, Luo YF. A comparative study on maximum power point tracking techniques for photovoltaic generation systems operating under fast changing environments. Sol Energy 2015;119:261–76.
[27] Liu YH, Chen JH, Huang JW. A review of maximum power point tracking techniques for use in partially shaded conditions. Sustain Energy Rev 2015;41:436–53.
[28] Hong Y, Pham SN, Yoo T, Chae K, Baek KH, Kim YS. Efficient maximum power point tracking for a distributed PV system under rapidly changing environmental conditions. Power Electron IEEE Trans 2015;30:4209–18.
[29] Zaniuri MAAM, Radzi MAM, Soh AC, Rahim NA. Development of adaptive perturb and observe-fuzzy control maximum power point tracking for photovoltaic boost dc–dc converter. Renew Power Gener IET 2014;8:183–94.
[30] Rajesh R, Mabel MC. Efficiency analysis of a multi-fuzzy logic controller for the determination of operating points in a PV system. Sol Energy 2014;99:77–87.
[31] Arulmurugan R, Suthanthiravanitha N. Model and design of a fuzzy-based Hopfield NN tracking controller for standalone PV applications. Electr Power Syst Res 2015;120:184–93.
[32] Zhou L, Chen Y, Guo K, Jia F. New approach for MPPT control of photovoltaic system with mutative-scale dual-carrier chaotic search. Power Electron IEEE Trans 2011;26:1038–48.
[33] Chen LR, Tsai CH, Lin YL, Lai YS. A biological swarm chasing algorithm for tracking the PV maximum power point. Energy Convers IEEE Trans 2010;25:484–93.
[34] Miyatake M, Veerachary M, Toriumi F, Fujii N, Ko H. Maximum power point tracking of multiple photovoltaic arrays: a PSO approach. Aerosp Electron Syst IEEE Trans 2011;47:367–80.
[35] Chao KH, Chen JP. A maximum power point tracking method based on particle swarm optimization for photovoltaic module arrays with shadows. ICIC Express Lett 2014;8:697–702.
[36] Ishaque K, Salam Z, Amjad M, Mekhilef S. An improved particle swarm optimization (PSO)-based MPPT for PV with reduced steady-state oscillation. Power Electron IEEE Trans 2012;27:3627–38.
[37] Liu YH, Huang SC, Huang JW, Liang WC. A particle swarm optimization-based maximum power point tracking algorithm for PV systems operating under partially shaded conditions. Energy Convers IEEE Trans 2012;27:1027–35.
[38] Kashif I, Zainal S, Amir S, Muhammad A. A direct control based maximum power point tracking method for photovoltaic system under partial shading conditions using particle swarm optimization algorithm. Appl Energy 2012;99:414–22.
[39] Kennedy J, Eberhart R. Particle swarm optimization. In: International neural networks conference on: IEEE; 1995. p. 1942–8.
[40] SANYO HIP 2717 Datasheet, <http://iris.nyit.edu/~mbertome/solardecathlon/SDClerical/SD_DESIGN+DEVELOPMENT/091804_Sanyo190HITBrochure.pdf>.
[41] Tang KH, Chao KH, Chao YW, Chen JP. Design and implementation of a simulator for photovoltaic modules. J Photoenergy Int 2012:1–6. Article ID 368931.
[42] Hart DW. Introduction to power electronics. New York: Prentice Hall; 2003.